Adhesion of metallic glass and epoxy in composite-metal bonding

Lee Hamill[1,*], Steven Nutt[1]

1. Department of Chemical Engineering and Materials Science, University of Southern California, Los Angeles, CA 90089, USA

Abstract:

We report the effects of surface preparation on the adhesive strength between a bulk metallic glass (BMG) alloy and carbon fiber reinforced epoxy. The motivation of the study was to explore the potential for BMG alloys to be laminated with carbon fiber (CF) composites in fiber metal laminates (FMLs), structures in which galvanic coupling with the metallic component (aluminum) generally precludes the use of CF composites. Select surface treatment methods were performed on both BMG and aluminum samples, and the surfaces were subsequently compared via scanning electron microscopy (SEM) and measurements of water contact angle (WCA) and roughness. Results of characterization experiments indicated that the BMG alloy responded to surface treatments much like aluminum, and that these treatment methods when applied to BMGs can promote adhesion. Lap shear tests were also performed to evaluate the bond quality at composite-metal interfaces. The bond strength at the BMG-composite interface was as strong or stronger than aluminum-composite interfaces, with the exception of samples pre-treated by anodization.

Key words: A. Prepreg, A. Carbon fibre, B. Adhesion, B. Surface Properties

Hamill L, Nutt S. Adhesion of metallic glass and epoxy in composite-metal bonding. Compos Part B 2018;134:186-192. DOI: https://doi.org/10.1016/j.compositesb.2017.09.044

1. Introduction

The aerospace industry constantly seeks materials that provide some benefit in performance and cost while minimizing or reducing weight. Aircraft companies in particular increasingly use composite materials in aircraft components. This shift has ameliorated concerns about fatigue issues normally associated with metallic aircraft while helping reduce aircraft weight and thus fuel costs. One composite-based structure deployed in recent commercial aircraft design is the fiber metal laminate (FML). FMLs consist of alternating layers of fiber-reinforced polymer (FRP) and metal. The most common commercial FML product, GLARE, consists of alternating layers of glass fiber-reinforced epoxy and aluminum. However, researchers have investigated the possibilities of using different composite and metal combinations. [1–7] One particular combination that has proven unfeasible is carbon fiber composite and aluminum because of the galvanic corrosion that results from contact between two materials of different electric potential. [8–12] Research efforts have aimed to reduce the galvanic corrosion of carbon fiber-aluminum FMLs by using barriers and coatings to isolate the two materials. [8,10,12] However, this combination of materials in FMLs has yet to achieve commercial viability.

Bulk metallic glass (BMG) presents one alternative to aluminum that can be paired with carbon fiber FRPs (CFRPs) in a FML structure and possibly avoid galvanic corrosion; BMGs resist corrosion because of the absence of grain boundaries in the microstructure. [13] BMGs exhibit other appealing attributes, including high hardness, strength, elastic limits, and impact resistance, making them candidates for certain high performance applications. [14–18] For example, recent reports have shown that BMGs are viable candidates for hypervelocity impact

shielding for spacecraft and satellites. [16,19] Weight is an especially critical consideration for space applications, as space structures must be as light as possible to minimize mission cost. FMLs offer an opportunity to leverage the intrinsic low density of FRPCs combined with the high hardness and impact resistance of BMGs.

The objective of this study was to evaluate the effects of surface treatments on adhesion between BMG and FRPs in an FML structure. Surface treatments commonly used on aluminum to promote adhesion were performed on BMG samples, and the resulting surfaces were characterized and compared to treated aluminum surfaces. The treatments selected mechanically and/or chemically altered the surface to promote adhesion. The metal surfaces in this study were evaluated by scanning electron microscopy (SEM), and surface roughness values and water contact angles were measured. For mechanical characterization, lap shear specimens were constructed and tested to determine the resulting bond strength at the composite-metal interface. In the presentation of results, we show that some of the surface treatments commonly used on aluminum also increase adhesive bonding for BMGs and CFRPs, demonstrating the potential to introduce FML designs that pair carbon fiber composites with corrosion resistant BMG alloys

2. Experimental Procedures

2.1 Materials and Curing Methods

Two alloys were selected for this study – a common precipitation-hardened aluminum alloy (Al 6061-T6) and a BMG alloy ($Zr_{44}Ti_{11}Ni_{10}Cu_{10}Be_{25}$). A carbon fiber reinforced epoxy prepreg,

consisting of a toughened epoxy (Cytec Industries, Inc. 5320-1) and a unidirectional (UD) carbon fiber tape, was chosen as the composite layer.

Adhesion samples were produced by co-curing, a method commonly used to produce FML components as well as in investigations of composite-metal adhesion. [20–23] During co-curing, the composite cures as it simultaneously bonds to the metal substrate, and excess resin from the composite prepreg serves as the adhesive between the two components. [20] Some samples included an added adhesive layer (3M Scotch-Weld Structural Adhesive Film AF 163-2) at the composite-metal interface to compare the adhesion that results from a bond with excess resin to a bond with added adhesive.

2.2 Material Surface Treatments

Researchers have evaluated the effects of various metal surface treatments on adhesion. [13,20,21,24–32] The basic objective when preparing a surface for adhesion is to maximize surface energy, and this can be achieved through several avenues. [31] For example, increasing surface roughness increases the surface energy of a substrate and provides mechanical interlocking between the substrate and polymer or adhesive, thus increasing bond strength. [24,31,33] A second way to increase surface energy and bond strength is to modify surface chemistry.[24]

Four surface conditions were investigated, including a control and three surface treatment methods. Prior to surface treatment, all metal surfaces were cleaned with a common degreaser, methyl ethyl ketone (MEK).[24,31] As a control, metal surfaces were not further treated after the degreasing stage. The first surface treatment method was simple mechanical abrasion, a means of

increasing surface roughness. [20,24,25] Metal samples were abraded with 80-grit abrasive using a hand-held orbital sander, followed by another round of degreasing with MEK prior to bonding.

Phosphoric acid anodizing (PAA) was used as the second surface treatment method.[34] Samples were initially degreased with MEK, then subjected to a sequence of electrochemical treatments. First, samples were immersed for 10 minutes in an FPL deoxidizing solution held at 65-71°C (ratio of 14 g sodium dichromate, 300 ml DI water, and 94 ml sulfuric acid). Following the FPL etch, samples were rinsed with DI water, then transferred to the anodizing solution (ratio of 400 ml DI water to 45 ml phosphoric acid). The bottom portion of each sample was submerged in the PAA solution, while the top portion of the sample was connected to the positive pole of an external power source. The negative pole was connected to a copper wire, which was immersed in the PAA solution. During the first three minutes of anodizing, the voltage of the power source was gradually increased to 15 V, and held constant for the remainder of the test. Each sample was anodized for a total of 20 minutes. After anodizing, the samples were rinsed with DI water and air dried. Anodizing was performed immediately prior to bonding.

In a third surface treatment method, a silane film was applied to sample surfaces, a method previously shown to promote polymer-metal adhesion, [21,28,29,35–37] including some BMG alloys.30 Samples were prepared following the procedure outlined by Wang and Gupta.[36] The silane solution consisted of 3 wt% silane (3-(Trimethoxysilyl)propyl methacrylate, Fischer Scientific) and 97% methanol. Initially, each sample was ground with 80 and 120 grit abrasive and subsequently degreased with MEK. The silane solution was then applied to each metal sample by pipette. After one minute, excess solution was shed, and the samples were cured in an oven for one hour at 110°C.

2.3 Characterization Methods

Select methods were used to characterize treated metal surfaces to compare the effects of each treatment on the two alloys. Characterization included measuring water contact angle and surface roughness and imaging by scanning electron microscope (SEM).

Water contact angle is a common measure used to analyze the potential for a surface to adhere to other substances, and has been used on both BMG and aluminum surfaces in the past. [38,39] The higher the energy of a surface, the more likely it is to form bonds with other substances to lower its energy. Therefore, a low contact angle (more spreading of the water) indicates a high surface energy, and a high contact angle (less spreading of the water) indicates a low surface energy. A measurement system (Rame Hart 290F1) was used to measure the contact angle for a water droplet on each treated surface. Tests were performed at 20 °C using 4 μL drops.

Profilometery was performed to measure the surface roughness of the samples using an optical surface profilometer (Zygo NewView 8000), and SEM was used to image sample surfaces before and after surface treatment. Electron micrographs were recorded with a low vacuum SEM (JEOL JSM-6610LV) in scanning electron imaging (SEI) mode at 20kV. Evaluation of surface chemistry was performed using x-ray photoelectron spectroscopy (XPS). XPS spectra were acquired using a photoelectron spectrometer (Kratos Ultra X-ray Photoelectron Spectrometer) with the analyzer lens in hybrid mode. A monochromatic aluminum anode was used to perform high resolution scans with a 5mA operating current, 10 kV voltage, 0.1 eV step size, and 20 eV pass energy. Pressure was maintained in the range 1-3 $\times$ 10^{-8} torr. Binding energies of the spectra were referenced to the C1s core level at 284.6 eV.

2.4 Lap Shear Preparation and Testing

Lap shear tests, commonly used to measure interface bond strength, were used in this study to evaluate the effect of each surface treatment on adhesion.[20–23,25,31,32,38,40,41] Sample preparation and testing were performed in accordance with ASTM D5868. Lap shear samples were produced by co-curing metal and composite pieces. Each metal piece was 25.4 × 101.6 × 1.5 mm, while composite pieces were produced by stacking four plies, each 25.4 × 101.6 mm. An individual lap shear sample was fabricated by combining one metal and one composite piece with a 25.4 mm overlap. Among the set of samples, surface treatment, processing method, and use of an adhesive film between the composite and metal were varied. For each surface treatment, 12 samples were produced. Of the 12 samples, six were cured in an autoclave, while the other six were cured by a vacuum bag only (VBO) method in an oven. Within each set of six, three samples included a single 25.4 × 25.4 mm film of adhesive (3M Scotch-Weld Structural Adhesive Film AF 163-2) between the metal and composite, while the other three did not.

Samples were cured on an aluminum tool plate and sealed with a vacuum bag, to which vacuum was applied during the cure cycle. The tool plate included a step of equal thickness to the metal (1.5 mm) to ensure that the composite lays flat as it cures, and edge dams were placed around each composite edge to maintain the shape of the composite and provide a pathway for the trapped air in the composite to evacuate (Figure 1a). Figure 1b shows the complete vacuum bag assembly. A vacuum bag sealed the system, and air was evacuated through a valve. Underneath the vacuum bag was a layer of porous breather, which allowed for even air evacuation. Finally, release film was included in between the composite prepreg and breather to prevent adhesion of the breather to the part. The manufacturer's recommended cure cycle was used: 3 hour dwell at 121

°C, 1.5 °C/minute ramp rate. Samples cured in the autoclave were cured under a pressure of 80 psi, while oven-cured samples were subject to atmospheric pressure. Lap-shear samples were tested in tension mode (INSTRON 5585H). Each end of the sample was gripped in fixtures with an initial grip separation of 75 mm, and load was applied with an extension rate of 13 mm/min. Upon failure, each surface was examined with a microscope (Dino-Lite Premier2 Digital Microscope) and classified as one or more of the failure modes outlined in ASTM D5573, a commonly practiced method for evaluating lap shear specimens.42,43 The percent area of each fracture surface corresponding to a particular failure mode was calculated using software (ImageJ). Representative images of each type of failure mode were recorded using a light microscope (Keyence VHX-5000).

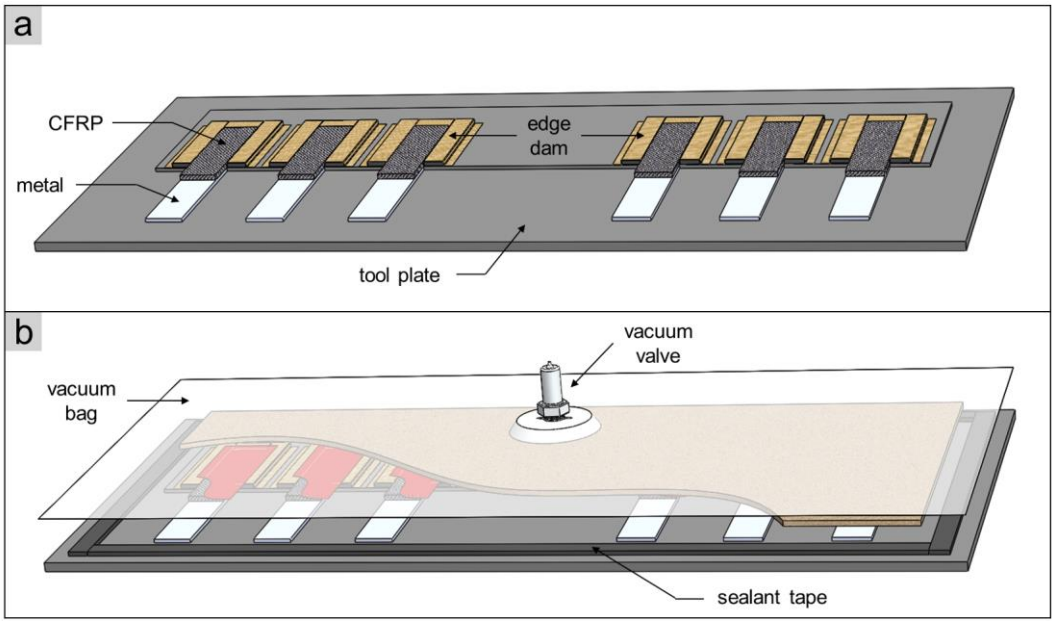

Figure 1: *Vacuum bag assembly for lap shear laminate manufacture. (a) The tool plate includes a step to ensure that the composite lays flat as it cures. Each lap shear sample with edge dam bordering the composite is shown. (b) Complete vacuum bag assembly including release film (red) and breather (brown) in between the samples and vacuum bag.*

3. Results and Discussion

3.1 Metal Surface Characterization

SEM micrographs (Figure 2) revealed the effects of surface treatments on the surface topography of BMG and aluminum alloys. In the control, the BMG sample was smooth, while the Al sample exhibited greater initial roughness (Fig 2a and 2b). Figure 2d shows that after abrasive grinding, the pattern of grooves on the Al surface remained, and the grooves appeared to be deeper. Abrasive grinding also produced grooves on the BMG surface (Figure 2c), although the grooves were shallower than the grooves on the Al surface for the same treatment, a consequence of the greater hardness of BMG alloys. This distinction indicates that abrasion time must be adapted to the specific BMG alloy.

PAA produced generally similar results for BMG and Al samples (Figures 2e and 2f), with a few key differences. Both samples exhibited a surface film, an oxide layer that typically forms when PAA is performed, indicating that PAA formed an oxide layer on BMG surfaces, much like it does on Al. XPS results confirmed the presence of zirconium oxide (peaks at 183 eV and 185.5 eV) on the anodized BMG surface and aluminum oxide (peak at 75 eV) on the anodized Al surface. However, although a film is observed on both samples, the appearance is distinct for the BMG and Al samples. The Al surface exhibits a uniform surface with pits, while the BMG surface exhibits a pattern of dried cracks and no observable depressions.

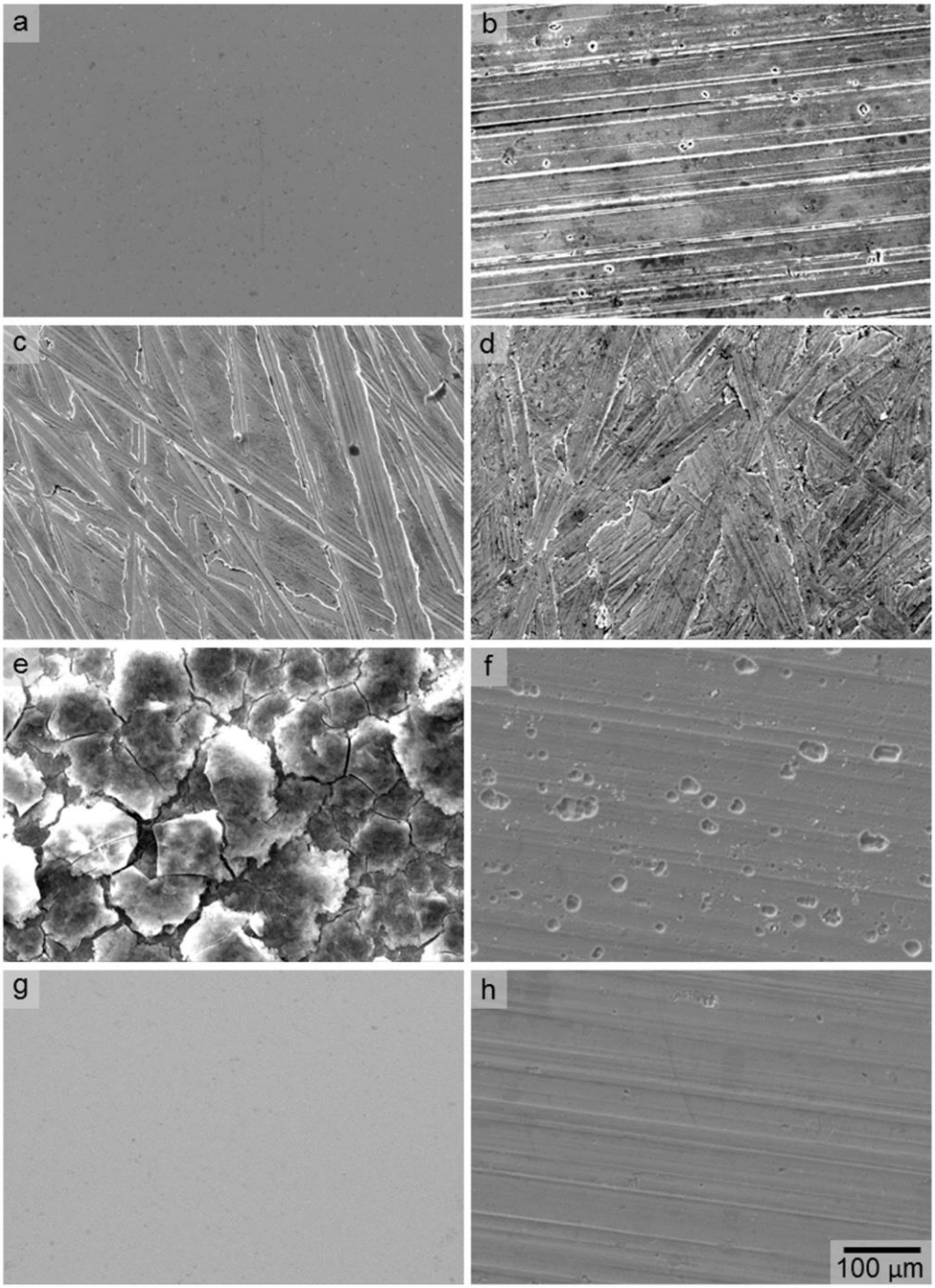

Figure 2: *SEM micrographs of treated metal surfaces. BMG samples are shown on the left with their Al counterparts on the right: (a) BMG control, (b) Al control, (c) BMG abrasion, (d) Al abrasion, (e) BMG PAA, (f) Al PAA, (g) BMG silane, and (h) Al silane. The scale bar shown is applicable to all parts of this figure.*

The surfaces of silane treated samples (Figures 2g and 2h) resembled those of the control samples. However, the grooves and surface defects on the control surfaces were not as apparent on silane treated samples, indicating that a film was formed on the surface. XPS revealed a peak at 102.1 eV and 102.5 eV for the treated aluminum and BMG surface, respectively, indicating the presence of organic silicon (expected peak ~102 eV). This confirmed the presence of a silane film on each surface. Aside from these minor distinctions, there were no significant differences between the control samples and the silane treated samples.

Water contact angle (Table 1) and surface roughness (Table 2) measurements provide quantitative support to the SEM observations. The BMG and Al control samples differed - as-received BMG samples were smooth (surface roughness of 0.146 μm), while the as-received Al samples were rougher (surface roughness of 0.462 μm). The difference was attributed to the processing method used to fabricate the samples. BMG samples were produced by casting, which produced a surface that replicated the mold surface. Casting molds typically have low surface roughness, so it is common for cast BMG alloys to have extremely smooth surfaces. Industrial Al sheet metal, on the other hand, is typically produced by high volume forming/grinding processes with higher tolerances on surface quality.

Table 1: *Water contact angle results.*

	Water Contact Angle (°)			
	Control	Abrasion	PAA	Silane
BMG ($Zr_{44}Ti_{11}Ni_{10}Cu_{10}Be_{25}$)	67.26 ± 3.63	32.68 ± 4.04	0.00 ± 0.00	61.13± 3.00
Al 6061 – T6	0.00 ± 0.00	0.00 ± 0.00	0.00 ± 0.00	72.87 ± 7.10

Abrasive grinding enhanced wetting in BMG samples. The WCA for BMG decreased from 67.26° in the control state to 32.68° after abrasive grinding. The Al samples, on the other hand,

yielded a WCA of 0° for both the control and abrasive ground states. Comparing WCA results to roughness data, additional factors contributed to the different wetting behavior of aluminum and BMG. Typically, the greater the surface roughness, the lower the WCA. However, when comparing the BMG abrasion sample to the Al control sample, the BMG abrasion sample exhibited a greater WCA, despite being rougher, indicating that factors other than roughness contribute to the WCA values. In general, the BMG alloy exhibited lower wettability (greater WCA) than Al samples.

Table 1: *Water contact angle results.*

	Surface Roughness (µm)			
	Control	Abrasion	PAA	Silane
BMG ($Zr_{44}Ti_{11}Ni_{10}Cu_{10}Be_{25}$)	0.146	0.786	0.438	0.539
Al 6061 – T6	0.462	1.683	0.448	0.717

The PAA treatment yielded WCA values of 0° for both BMG and Al. Roughness values for the PAA treated BMG and Al samples were also similar - 0.438 µm and 0.448 µm, respectively. The purpose of PAA treatment was to achieve a roughened as well as a chemically altered surface. Chemical modification to the surface is the primary factor responsible for the increased wettability - the WCAs for both BMG and Al were reduced to 0° after PAA treatment, while the surface was less rough than it was after abrasive grinding in each case.

Finally, silane treatment did not substantially increase wettability or roughness of either the BMG or Al surface. WCA values for silane-treated BMG and Al samples were 61.13° and 72.87°, respectively. The WCA for Al increased compared to all other states, indicating that the silane film was more hydrophobic than the Al surface. Roughness values for silane-treated BMG and Al surfaces were 0.539 µm and 0.717 µm, respectively.

3.2 Lap Shear Results

Figure 3 shows the results of lap shear tests, organized in groups corresponding to the surface treatment used on the metal and whether or not an adhesive film was included (indicated by an "A"). Within each group, the average peak load is shown for each metal type and processing method. In all cases except for PAA, BMG samples yielded peak load values that matched or exceeded those of Al samples for each set of conditions. The results indicate that the BMG can be a viable substitute for aluminum in future FMLs and in applications involving metal-to-composite co-curing. In addition, samples that included an adhesive film yielded greater values of peak load than samples without an adhesive film. Samples with adhesive achieved the same approximate

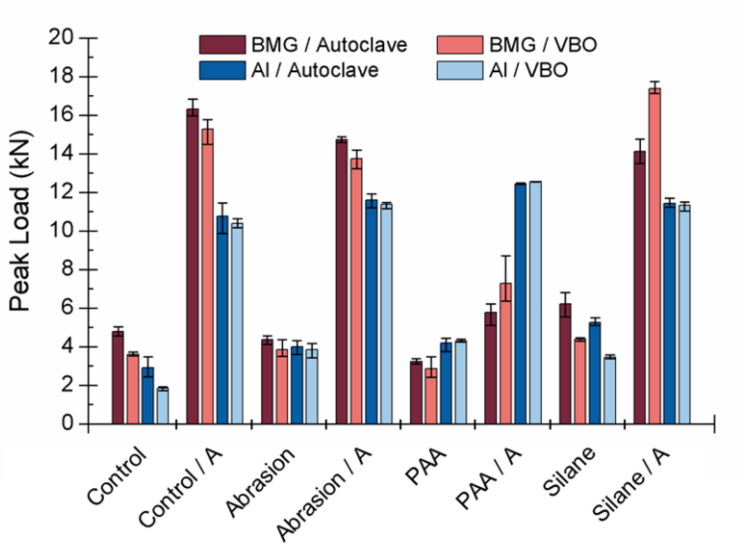

Figure 3: *Peak load values of lap shear samples tested in tension. Each column height is the average of three identically produced samples with the standard deviation shown through error bars. Results are grouped by surface treatment method, with the letter "A" indicating that an adhesive film was used. Within each group, metal type and processing method are separated.*

peak load for both alloys, regardless of the surface treatment, indicating that in this case, at least, the intrinsic performance of the adhesive outweighs the benefits obtained from a particular surface treatment.

There was no consistent trend in peak load when comparing the results of samples processed by VBO and autoclave methods. In some cases, VBO samples resulted in greater peak loads than autoclave samples, while in others the reverse was true. In most cases, differences in adhesive strength fell within the error for each result, and thus the two processing methods yielded no significant differences.

3.3 Failure Classification

Sample failure modes were classified according to ASTM 5573 and included adhesive, thin layer cohesive, light fiber tear, fiber tear, and stock break (Figure 4). Adhesive failure refers to a clean failure at the metal-polymer interface with no polymer residue at the metal surface, and indicates a weak interface bond that typically corresponds to lower peak load values. Thin layer cohesive failure indicates a slightly stronger bond than adhesive failure, and is identified by a thin layer of polymer or adhesive remaining on the metal surface upon failure. Sample surfaces were classified as light fiber tear failure mode if a thin layer of polymer was transferred to the metal surface along with a small amount of fibers. If failure occurred exclusively below the composite surface, and fibers were observed across the entire metal side of the failure surface, the failure mode was designated as fiber tear. Finally, stock break failure mode was assigned to samples in which failure did not occur along the bond line, but instead resulted in failure of the metal.

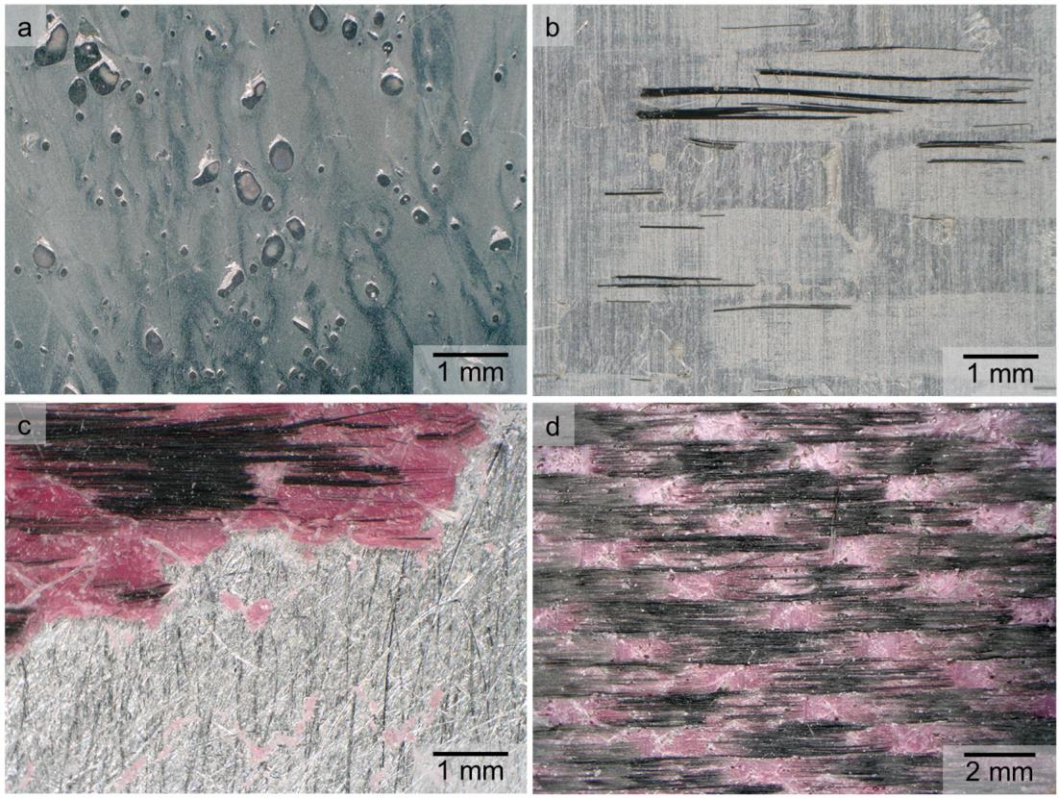

Figure 4: *Microscope images of fracture surfaces of the metal: (a) combination of adhesive and thin layer cohesive failure on a BMG surface, (b) combination of thin layer cohesive and light fiber tear on an aluminum surface, (c) combination of adhesive and fiber tear on an aluminum surface, and (d) fiber tear on a BMG surface.*

A summary of the failure classification results is shown in Table 3. Each sample exhibited either (a) a combination of adhesive, thin layer cohesive, and light fiber tear, or (b) a combination of adhesive, fiber tear, and light fiber tear. Because the boundary between thin layer cohesive and light fiber tear failure modes was difficult to reliably and accurately locate, these two failure modes are combined into a single percent area value. Similarly, the difference between fiber tear and light fiber tear was subtle, so for samples that exhibited this combination of failure modes, fiber tear and light fiber tear also were combined into a single percent area value. Percent area

values were calculated by outlining the region of interest in a fracture surface image and calculating the percent area of the surface that that section comprised.

Table 3: *Overview of failure modes observed on the failure surface of lap shear samples. The letter "A" indicates that an adhesive film was used in the lap shear sample.*

		Adhesive	Thin Layer Cohesive / Light Fiber Tear	Fiber Tear / Light Fiber Tear	Stock Break
Control	Al	24%	76%	--	--
	BMG	72%	28%	--	--
Control / A	Al	50%	--	50%	--
	BMG	--	--	100%	--
Abrasion	Al	--	100%	--	--
	BMG	45%	55%	--	--
Abrasion / A	Al	22%	--	78%	--
	BMG	1%	--	99%	--
PAA	Al	2%	98%	--	--
	BMG	59%	41%	--	--
PAA / A	Al	--	--	50%	50%
	BMG	100%	--	--	--
Silane	Al	15%	85%	--	--
	BMG	48%	52%	--	--
Silane / A	Al	30%	--	70%	--
	BMG	--	--	100%	--

All samples that did not include a layer of adhesive film at the composite-metal interface resulted in a combination of adhesive, thin layer cohesive, and light fiber tear failure modes. These failure modes, which indicate weak bonds, were consistent with the low peak load values exhibited by samples with no adhesive layer. On average, in BMG samples without adhesive, 56% of the failure surface was classified as adhesive, while in aluminum samples without adhesive, 10% was classified as such. This finding indicates that the epoxy in the prepreg bonded more readily to aluminum than to BMG.

Surface treatment of the BMG samples resulted in failure modes indicative of stronger bonds. The BMG control samples resulted in 72% adhesive failure, while those treated by abrasion, PAA, and silane exhibited ~50% adhesive failure. Aluminum samples exhibited a similar decrease in adhesive failure after surface treatment, but a lower percent area covered by adhesive failure overall relative to BMG.

The failure modes observed in samples that included an adhesive film indicated stronger bonding, in accord with lap shear test results. Overall, in BMG samples with adhesive, 75% of the failure area was characterized by light fiber tear and fiber tear, while only 25% area exhibited adhesive failure. The Al samples with adhesive film yielded failure modes similar to those without adhesives. While the percent area covered by adhesive failure increased slightly to 25%, the remaining 75% exhibited light fiber tear and fiber tear, as well as some stock-break failure, indicating that bonding was overall stronger, and in some cases, stronger than the aluminum itself.

Closer examination of the results of the individual surface treatment methods provides support to the conclusion from the lap shear results that the BMG samples with the added adhesive layer exhibited stronger bonding than aluminum counterparts. The BMG control samples in this category yielded 0% adhesive failure, while the aluminum samples resulted in 50% adhesive failure. Similarly, silane treated BMG samples produced 0% adhesive failure, while the silane treated aluminum samples resulted in 30% adhesive failure. An exception to the conclusion that BMG samples produced stronger bonding than aluminum is evident in the PAA surface treatment. BMG samples with this surface treatment resulted in 100% adhesive failure, while aluminum PAA samples exhibited 0% adhesive failure. This distinction is reflected in the lower bond strength

measured in lap shear tests and indicates that the PAA treatment method must be altered either chemically or in application when performed on BMG alloys.

4. Conclusions

Using surface treatments that are well-established for aluminum alloys, we have determined the effectiveness of these treatments on the adhesive bond strength between BMG alloys and polymer matrices in composites. While the methods chosen for surface treatment produced BMG surfaces similar to treated aluminum surfaces, intrinsic differences in the surface chemistry of the two alloys contributed to differences in adhesion behavior. Lap shear results along with analysis of the failure surfaces confirmed that under shear loading conditions, BMG samples exhibited peak loads that matched or exceeded those of aluminum samples in all cases except for those that were anodized. The latter distinction indicates that a different anodization recipe will be required for BMG alloys.

Commercial FMLs are currently restricted to aluminum/glass-fiber-epoxy composite combinations, primarily for two reasons: (1) to avoid galvanic corrosion between the metal and composite layer, and (2) aluminum is readily available in sheet metal form. BMGs are highly resistant to corrosion because of their non-crystalline microstructure and lack of grain boundaries. The use of BMGs in FMLs could potentially eliminate the issue of galvanic corrosion and open the design space to CFRPs, thereby leveraging both the superior performance of CFRPs (relative to GFRPs), and of BMGs (relative to Al alloys). In addition, BMG production has long been restricted to melt-spun ribbons less than 0.5 mm thick, or small castings of BMG, yielding thickness greater than 1 mm. These processes were not suitable for production of large sheets of

BMG required for FMLs. However, recent efforts to produce BMG sheets by twin-roll casting have demonstrated production of sheet stock with thicknesses of 0.1 – 1 mm 44, potentially enabling larger scale production of BMG-based FMLs.

This study is the first to evaluate the adhesion at BMG-composite interfaces and compare it to the interface currently present in commercial FMLs. The results indicate that BMG is a viable option for structures that involve composite to metal co-curing and bonding. While the high cost of BMG may preclude use in commercial aircraft, the results support the use of BMG-based FMLs for structural applications in which the superior mechanical properties of BMG yield distinct benefits. One application in particular for which BMG-FMLs are being considered is spacecraft shielding. BMGs have been shown to provide effective protection against hypervelocity impact from micro-meteorites and debris, both of which constitute serious threats to spacecraft. FMLs present an opportunity to leverage the high strength and hardness properties of BMGs while minimizing weight through the incorporation of composite material in a laminate structure. Results of this study demonstrate the possibility for BMGs to be bonded to composite materials in this way.

Acknowledgements: This research was supported by the M.C. Gill Composites Center and NASA SBIR Z2.01. Solvay Inc, Airtech International, and Liquidmetal Technologies donated prepreg, consumable materials, and BMG samples, respectively. Zygo Corporation provided access to their optical profilometer. Assistance on the project was provided by Karissa Hendrie, and Dr. Timotei Centea provided guidance to the project.

References:

[1] Cortés, P. & Cantwell, W. J. Structure–properties relations in titanium-based thermoplastic fiber metal laminates. *Polym. Compos.* **27,** 264–270 (2006).

[2] Cantwell, W. J. & Cortes, P. The fracture properties of a fibre – metal laminate based on magnesium alloy. *Compos. Part B* **37,** 163–170 (2006).

[3] Abdullah, M. R. & Cantwell, W. J. The impact resistance of fiber–metal laminates based on glass fiber reinforced polypropylene. *Polym. Compos.* **27,** 700–708 (2006).

[4] Langdon, G. S., Nurick, G. N., Karagiozova, D. & Cantwell, W. J. Fiber-Metal Laminate Panels Subjected to Blast Loading. in *Dynamic Failure of Materials and Structures* 269–296 (2010). doi:10.1007/978-1-4419-0446-1

[5] Khan, S. U., Alderliesten, R. C. & Benedictus, R. Delamination in Fiber Metal Laminates (GLARE) during fatigue crack growth under variable amplitude loading. *Int. J. Fatigue* **33,** 1292–1303 (2011).

[6] Sinmazçelik, T., Avcu, E., Bora, M. Ö. & Çoban, O. A review: Fibre metal laminates, background, bonding types and applied test methods. *Mater. Des.* **32,** 3671–3685 (2011).

[7] Du, D., Hu, Y., Li, H., Liu, C. & Tao, J. Open-hole tensile progressive damage and failure prediction of carbon fiber-reinforced PEEK-titanium laminates. *Compos. Part B Eng.* **91,** 65–74 (2016).

[8] Wang, W. X., Takao, Y., Kashima, I. & Matsubara, T. CFRP/Al-FRML Based on Nano-composite Coating and Its Mechanical Properties. in *48th AIAA/ASME/ASCE/AHS/ASC Structures, Structural Dynamics, and Materials Conference – 15th – April 23-26, 2007 – Honoloulu, HI* (2007). doi:10.2514/6.2007-2268

[9] Xue, J., Wang, W., Takao, Y. & Matsubara, T. Reduction of thermal residual stress in carbon fiber aluminum laminates using a thermal expansion clamp. *Compos. Part A* **42,** 986–992 (2011).

[10] Wang, W. *et al.* Development of galvanic corrosion-resistant CFML based on composite coating. *J. Soc. Mater. Sci.* **56,** 420–425 (2007).

[11] Asundi, A. & Choi, A. Y. N. Fiber Metal Laminates: An Advanced Material for Future Aircraft. *J. Mater. Process. Technol.* **63,** 384–394 (1997).

[12] Vermeeren, C. A. J. R. *Application of Carbon Fibers in ARALL Laminates - Report LR-658*. (1991).

[13] Gebert, A. *et al.* Investigations on the electrochemical behaviour of Zr-based bulk metallic glasses. *Mater. Sci. Eng. A* **267,** 294–300 (1999).

[14] Johnson, W. L. Bulk Glass-Forming Metallic Alloys: Science and Technology. *MRS Bull.* **24,** 42–56 (1999).

[15] Hofmann, D. C. *et al.* Designing metallic glass matrix composites with high toughness and tensile ductility. *Nature* **451,** 1085–1089 (2008).

[16] Hamill, L. *et al.* Hypervelocity Impact Phenomenon in Bulk Metallic Glasses and Composites. *Adv. Eng. Mater.* **16,** 85–93 (2014).

[17] Salimon, A. I., Ashby, M. F., Bréchet, Y. & Greer, A. L. Bulk metallic glasses: what are they good for? *Mater. Sci. Eng. A* **375–377,** 385–388 (2004).

[18] Chuang, M.-H. *et al.* Mechanical properties and microstructure of Zr-Ti-Ni thin film metallic glasses modified with minor SF 6. *Compos. Part B Eng.* **129,** 243–250 (2017).

Hamill L, Centea T, Nutt S. Surface Porosity During Vacuum Bag-Only Prepreg Processing: Causes and Mitigation Strategies. Compos Part A Appl Sci Manuf 2015;75:1-10. DOI: doi:10.1016/j.compositesa.2015.04.009

[19] Hofmann, D. C., Hamill, L., Christiansen, E. & Nutt, S. Hypervelocity Impact Testing of a Metallic Glass-Stuffed Whipple Shield. *Adv. Eng. Mater.* **17,** 1313–1322 (2015).
[20] Shin, K. C., Lee, J. J. & Lee, D. G. A study on the lap shear strength of a co-cured single lap joint. *J. Adhes. Sci. Technol.* **14,** 123–139 (2000).
[21] Kim, W.-S. & Lee, J.-J. Adhesion strength and fatigue life improvement of co-cured composite/metal lap joints by silane-based interphase formation. *J. Adhes. Sci. Technol.* **21,** 125–140 (2007).
[22] Shin, K. C. & Lee, J. J. Tensile load-bearing capacity of co-cured double lap joints. *J. Adhes. Sci. Technol.* **14,** 1539–1556 (2000).
[23] Shin, K. C. & Lee, J. J. Fatigue characteristics of a co-cured single lap joint subjected to cyclic tensile loads. *J. Adhes. Sci. Technol.* **16,** 347–359 (2002).
[24] Molitor, P., Barron, V. & Young, T. Surface treatment of titanium for adhesive bonding to polymer composites: a review. *Int. J. Adhes. Adhes.* **21,** 129–136 (2001).
[25] Aktas, A. & Polat, Z. Improving Strength Performance of Adhesively Bonded Single-lap Composite Joints. *J. Compos. Mater.* **44,** 2919–2928 (2010).
[26] Malpass, B. W., Packham, D. E. & Bright, K. A Study of the Adhesion of Polyethylene to Porous Alumina Films Using the Scanning Electron Microscope. *J. Appl. Polym. Sci.* **18,** 3249–3258 (1974).
[27] Packham, D. E., Bright, K. & Malpass, B. W. Polyethylene to Aluminium. *J. Appl. Phys.* **18,** 3237–3247 (1974).
[28] Tanoglu, M., Mcknight, S. H., Palmese, G. R. & Gillespie, J. W. Use of silane coupling agents to enhance the performance of adhesively bonded alumina to resin hybrid composites. *Int. J. Adhes. Adhes.* **18,** 431–434 (1998).
[29] Jang, J. & Kim, E. U. I. K. Corrosion Protection of Epoxy-Coated Steel Using Different Silane Coupling Agents. *J. Appl. Polym. Sci.* **71,** 585–593 (1999).
[30] Yang, J. & Dauskardt, R. H. Hybrid coupling layers for bulk metallic glass adhesion. *J. Mater. Res.* **28,** 3164–3169 (2013).
[31] Molitor, P. & Young, T. Adhesives bonding of a titanium alloy to a glass fibre reinforced composite material. *Int. J. Adhes. Adhes.* **22,** 101–107 (2002).
[32] He, P., Chen, K. & Yang, J. Surface modifications of Ti alloy with tunable hierarchical structures and chemistry for improved metal-polymer interface used in deepwater composite riser. *Appl. Surf. Sci.* **328,** 614–622 (2015).
[33] Kinloch, A. J. Review: The science of adhesion. *J. Mater. Sci.* **15,** 2141–2166 (1980).
[34] Liu, C. *et al.* Interlaminar failure behavior of GLARE laminates under short-beam three-point-bending load. *Compos. Part B Eng.* **97,** 361–367 (2016).
[35] Lim, A. S., Melrose, Z. R., Thostenson, E. T. & Chou, T. Damage sensing of adhesively-bonded hybrid composite/steel joints using carbon nanotubes. *Compos. Sci. Technol.* **71,** 1183–1189 (2011).
[36] Wang, X. & Gupta, V. Construction and characterization of chemically joined stainless steel/E-glass composite sections. *Mech. Mater.* **37,** 1198–1209 (2005).
[37] Lee, C. Y., Bae, J.-H., Kim, T.-Y., Chang, S.-H. & Kim, S. Y. Using silane-functionalized graphene oxides for enhancing the interfacial bonding strength of carbon/epoxy composites. *Compos. Part A Appl. Sci. Manuf.* **75,** 11–17 (2015).
[38] Ochoa-Putman, C. & Vaidya, U. K. Mechanisms of interfacial adhesion in metal – polymer

composites – Effect of chemical treatment. *Compos. Part A* **42,** 906–915 (2011).
[39] Zhang, X., Sun, B., Feng, W., Zhang, Q. & Li, Q. Wetting Behavior of Polymer Melts on Bulk Metallic Glasses. *Appl. Mech. Mater.* **404,** 25–31 (2013).
[40] Liu, S. *et al.* An investigation of hygrothermal effects on adhesive materials and double lap shear joints of CFRP composite laminates. *Compos. Part B Eng.* **91,** 431–440 (2016).
[41] Chowdhury, N. M., Chiu, W. K., Wang, J. & Chang, P. Experimental and finite element studies of bolted, bonded and hybrid step lap joints of thick carbon fibre/epoxy panels used in aircraft structures. *Compos. Part B Eng.* **100,** 68–77 (2016).
[42] Ribeiro, T. E. A., Campilho, R. D. S. G., da Silva, L. F. M. & Goglio, L. Damage analysis of composite-aluminium adhesively-bonded single-lap joints. *Compos. Struct.* **136,** 25–33 (2016).
[43] Tamborrino, R. *et al.* Assessment of the effect of defects on mechanical properties of adhesive bonded joints by using non destructive methods. *Compos. Part B Eng.* **91,** 337–345 (2016).
[44] Hofmann, D. C., Roberts, S. & Johnson, W. L. Twin Roll Sheet Casting of Bulk Metallic Glasses and Composites in an Inert Environment. 18 (2012).